Cementitious materials containing nano-carriers and silica for the restoration of damaged concrete-based monuments

*Monica Tonelli [a,b§], Rita Gelli [a,b§], Rodorico Giorgi [a,b], Maria Isabella Pierigè [c], Francesca Ridi [a,b] * and Piero Baglioni [b] **

a. *Department of Chemistry "Ugo Schiff", University of Florence, via della Lastruccia, 3 Sesto Fiorentino (FI) 50019, Italy*

b. *CSGI, University of Florence, via della Lastruccia, 3 Sesto Fiorentino (FI) 50019, Italy*

c. *Soprintendenza Archeologia Belle Arti e Paesaggio per le province di Chieti e Pescara – MiBACT, Via degli Agostiniani, 14, Chieti 66100, Italy*

§These authors contributed equally to the manuscript.

*Corresponding authors:
E-mail: piero.baglioni@unifi.it, CSGI, University of Florence, Sesto Fiorentino (FI) 50019, Italy - Tel: +39-055-4573033 E-mail: francesca.ridi@unifi.it, Department of Chemistry "Ugo Schiff" & CSGI, University of Florence, Sesto Fiorentino (FI) 50019, Italy - Tel: +390554573015

Highlights

- Cement-based formulations to address different types of damages were developed;

- Several properties of the materials were optimized, according to the specific damage;

- A complete characterization revealed the potential of the developed formulations;

- Halloysite nanotubes loaded with benzotriazole were included in repair cementitious materials;

- The developed repair materials were applied on a War Memorial historical monument.

Abstract

The conservation of damaged concrete-based monuments is a demanding challenge for the contemporary world of cultural heritage, given the great number of historic concrete-based monuments built in the last century that are prone to continuous damages. In this work, we developed three different cement-based formulations to address the repair of diverse type of damages that affect these structures, *i.e.* delamination problems and cracks of different size. Formulations were improved with various additives, in order to obtain an easy application, a good workability of the paste and a proper setting time, according to the specific application. Silica was included in the formulations to enhance the adhesion to old concrete substrates, whereas halloysite nanotubes loaded with a corrosion inhibitor were also incorporated in the repair materials, to address in an innovative way the problem of corrosion of steel rebars. The formulations were characterized with a multi-technique approach, which allowed us to get a complete overview of the physico-chemical features of these repair materials. In addition, the adhesion of the formulations to old concrete substrates was investigated, as well as the release of the corrosion inhibitor within the cement matrix. Given the promising results obtained, the formulations were

applied at the War Memorial of Torricella Peligna (Italy), confirming their great potentialities in the field of historic concrete-based monuments conservation.

Graphical abstract
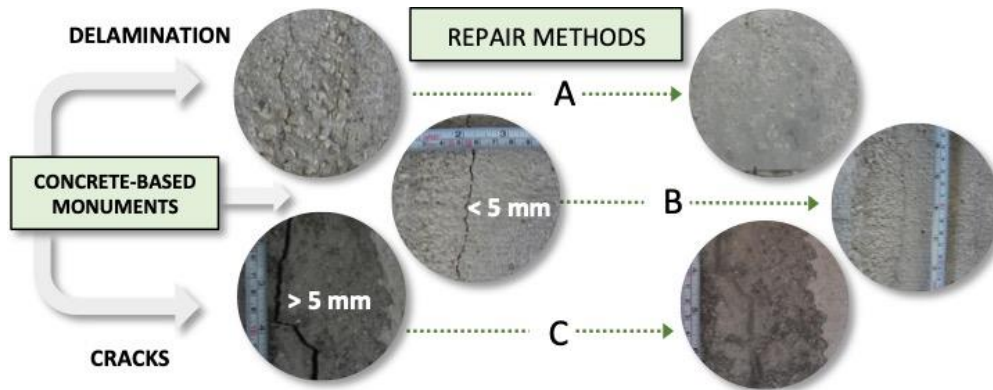
Keywords

Historic concrete; Cement; Conservation; Delamination; Cracks; Halloysite.

1. Introduction

Since the Roman times, cementitious materials are among the most produced materials all over the world, and nowadays reinforced concrete is the most widely used for construction purposes [1,2]. Concrete also represents the main building material of tangible cultural heritage during the 20th Century, as confirmed by the number of concrete-based monuments in the UNESCO World Heritage List [3]. Nevertheless, historic concrete is at risk. Unlike other traditional materials, concrete does not have well developed, universally implemented conservation methodologies for its investigation, repair or long-term maintenance [4–7]. The rapid deterioration of cement-based materials, strongly related to the surrounding environments, involves considerable resources to repair deteriorated structure, and one of the main factors affecting the durability of concrete is the surface permeability [8–12]. The complex network of pores of dried cementitious materials allows

4

for the ingress of potentially dangerous substances, leading to deterioration and influencing the long-term performance durability [13,14]. Beside all the strategies that can be used to prevent damages [15,16], it is also fundamental to develop effective methodologies to repair concrete-based structures when damages take place. As a matter of fact, delamination problems and cracks occurrence, allowing for an accelerated ingress of water and harmful substances (chlorides, CO_2, acids, alkalies and sulfates), can fasten the major physical and chemical degradation processes affecting concrete structures, such as the corrosion of steel rebars and the deterioration due to freezing and thawing processes [13]. Usually, when repair tasks are required, the 'Patch Repair Method' can be used, consisting in replacing deteriorated concrete from small areas with repairing mortars, paying attention to durability, material compatibility and structural performance [6]. Among all the possibilities to restore and enhance the service life of infrastructures, cement-based materials can act as a physical barrier to the penetration of water, ions and gases. The development of cement formulations enriched with inorganic admixtures for the achievement of additional benefits is an innovative approach to face the conservation of degraded cement-based historical monuments. It was recently reported in the literature that the addition of silica improves the microstructure of hydration products, refines the pore structure and densifies the interphase of the patch/surface, leading to less shrinkage and lower permeability [17]. The optimal choice for the improvement of the attachment at the interphase is nano-silica, due to its very high surface area and reactivity [18]. However, due to toxicity problems, it is important to consider different silica sources. Further on that, taking into account that the corrosion of steel reinforcement due to chloride ions is the primary cause of structures weakening [19], the inclusion of corrosion inhibitors into the formulations seems a convenient additional benefit for the enhancement of damaged structures lifetime. In particular, the use of smart carriers to achieve a controlled release

of inhibitors and to prolong the protective effect of these molecules was already reported in the literature [20–22]. Among the variety of carriers used to load and release corrosion inhibitors, nanotubular aluminosilicate clays such as halloysites (HNT) are a promising solution, being perfectly compatible with the chemical nature of the evolving phases commonly present in a cement paste [23,24], and combining the fibrous nature which can in principle improve the mechanical properties of the material with the presence of an empty lumen that can be loaded with active molecules [21,25–27].

In this work, we studied various cementitious formulations to be used for the restoration of damaged cement-based structure. The formulations here presented were ideated to recover small damages, such as delamination and cracks (< 1 cm), not affecting the structural performances but accelerating the general degradation of the buildings by allowing a faster ingress of harmful substances. We evaluated the use of several batches of silica, to reduce the cost of the materials and the hazards connected with the use of nano-particles while ensuring a good attachment of the coating to the surface to be recovered. The formulations were improved with various additives, to obtain an easy application, a good workability of the paste, and a proper setting time. HNTs loaded with corrosion inhibitors were also incorporated into the formulations, proving that smart nano-carriers can be also included into these formulations to achieve additional benefits. In particular, we decided to load HNTs with benzotriazole (BTA) as corrosion inhibitor, since its use is a generally recognized strategy to prevent chloride-induced corrosion [25,28,29]. The formulations were optimized depending on the final use and we selected three specific problems to be addressed: *i.* delamination of the surface; *ii.* very small cracks, where the use of sand is prevented; *iii.* big cracks or small aesthetic detachments. As a result, we identified three main formulations:

6

- Formulation A: a fluid cement paste that can be applied as a coating, to be used in case of delamination problems.

- Formulation B: a viscous cement paste, which can be easily injected, to be used in small cracks (width < 5 mm).

- Formulation C: a plastic repair mortar, suggested for big cracks (width 5-10 mm) or as repair mortar for small detachments.

Research aim

Surface damages in cement-based monuments typically include cracks and delamination issues, arising from multiple factors strongly related to the surrounding environment. Although concrete represents the main building material of tangible cultural heritage during the 20th Century, its conservation methodology is not well developed yet. Beside all the strategies that can be used to repair the structures, the use of cement-based materials not only preserves the monument appearance but can also act as a physical barrier, to prevent future damages. In order to address some of the common problems of damaged concrete monuments, here we developed three cement formulations, enriched with inorganic admixtures, to be used in case of delaminations (formulation A), cracks with thickness below 5 mm (formulation B) and cracks with thickness of 5 – 10 mm or small detachments (formulation C).

2. Materials and methods

2.1 Materials

All formulations were prepared using Portland cement (PC) CEM I 42.5 R from Knauf, HNT nanotubes from Imerys (extracted from a deposit in New Zealand, density 2.55 g/cm^3, specific

surface area 20 m^2/g as from technical datasheet) and SiO$_2$, either from Elkem (silica fume grade 940, surface area 20 m^2/g, measured by means of a Coulter SA 3100 analyser) or from Microbeton (poz/h fly ash, surface area 2.22 m^2/g). The sand used to prepare the formulations was purchased from SATAF (siliceous sand SATAF IMPALPABILE, SiO$_2$ 83-86 %, granulometry 0-0.2 mm), whereas the sand employed in the preparation of mortars for the applications of the coatings was CEN-Normsand DIN EN 196-1 obtained from Normensand. The superplasticizer Viscocrete was purchased from Sika. Methylhydroxyethyl cellulose (Culminal MHEC) was obtained from Hercules Inc., it has an average degree of substitution (DS) of 1.76, and the molar degree of substitution is 0.28. The anti-shrinkage agent Espandex 2000 was provided by Sika. For the loading of HNT, benzotriazole (BTA, purity > 99 %) was purchased from Sigma-Aldrich and Acetone (technical grade) from Carlo Erba. Deionized water was used for all the experiments.

2.2 Samples preparation

The samples described in this work were prepared by separately mixing the powders (cement, HNTs, sand, silica, Culminal) and the liquids (Espandex, Viscocrete, water), according to the different formulations. The compositions of the preliminary samples investigated are reported in Table S1 (effect of admixtures and SiO$_2$ from Elkem) and Table S2 (effect of admixtures and SiO$_2$ from Microbeton). On the basis of the obtained workability, setting time and adhesion, three final formulations (A, B and C) were selected (see the discussion in section 3.1), and their composition is reported in Table 1.

Table 1. Composition of the three selected formulations. Cement pastes A and B were prepared without sand, while mortar C was prepared using sand SATAF.

Sample	Cement (g)	Sand (g)	Silica (g)	HNT (g)	Culminal (g)	Espandex (g)	Viscocrete (g)	Water (g)	HNT wt %[1]	w/b[2]
A	8	-	0.333	0.833	0.021	0.20	0.0833	2.67	10	0.33
B	8.2	-	0.170	0.837	0.021	0.20	0.042	2.73	10	0.33
C	3.27	9.81	0.067	0.334	0.017	-	0.150	2.23	10	0.70

[1] weight percentage of HNT with respect to weight of cement + silica

[2] weight percentage of water with respect to weight of the binder, cement + silica

As a general protocol, the liquid mixture was slowly incorporated to the powder component and mixed with a spatula until a workable paste was obtained. After preparation, the formulations were transferred in different molds, according to the experiment to be performed, and cured at 25 °C and RH 98%. Specimens were lyophilized after 7 and 28 days to stop the hydration, for the characterization by means of scanning electron microscopy, X-rays diffraction, thermogravimetry and gas porosimetry.

Furthermore, some mortar specimens were prepared to be used as a surface for the application of fresh formulations as coatings. These mortars were prepared mixing PC and sand (Normensand, see 2.1) at a sand/cement (s/c) ratio of 3, along with a water/cement (w/c) ratio of 0.5. Mortar samples were cured in cylindrical molds (r = 0.7 cm, h = 0.5 cm) at 25 °C and RH 98% for at least 28 days. The surface of the mortars was then roughened with abrasive paper (P180) just before the application of the coating, to increase the contact area with the coating.

2.3 Loading of HNT with BTA

30 g of HNTs were mixed as a dry powder with 700 mL of a saturated solution of benzotriazole in acetone (86 mg/mL). The suspension was then evacuated using a vacuum pump, kept under

vacuum at p < 20 mbar for 3 h, cycled back to atmospheric pressure and kept in these conditions for 1 h. Afterwards, the suspension was again kept at p < 20 mbar for 1 h, and cycled back to atmospheric pressure for 1 h. The latter cycle was repeated, so to enhance the loading efficiency. Finally, HNTs were separated from solution by centrifugation, washed with water and dried overnight at 70 °C.

2.4 Methods

2.4.1 Scanning Electron Microscopy (SEM)

SEM images were collected on freeze-dried fracture surfaces with a field-emission ΣIGMA microscope (Carl Zeiss Microscopy). The used accelerating potential was 5.00 kV, while the working distance ~ 7 mm. The images were acquired with secondary electrons.

2.4.2 X-Rays Diffraction (XRD)

X-ray diffractograms on the freeze-dried and grinded powders were recorded with a D8 Advance with DAVINCI design (Bruker), operating at 40 kV and 40 mA, with a Cu source (emitting radiation λ=1.54 Å). Data were collected in the 5-70° 2θ range, with an increment of 0.03° and a time per step of 0.5 s.

2.4.3 Thermogravimetry (TGA)

Thermogravimetry analyses were performed by means of a STD Q600 instrument (TA Instruments), operating from room temperature to 1000 °C at 10 °C/min in nitrogen flux (100 mL/min). The freeze-dried samples were grinded and placed in alumina pans for the analysis.

2.4.4 Gas porosimetry

The Specific Surface Area (SSA) and Pore Size Distribution (PSD) of the powders was measured by means of a Coulter SA 3100 analyzer (Beckman Coulter), using nitrogen as adsorptive gas.

Before the measurements, the freeze-dried samples were grinded and outgassed for 1 h at 70 °C. Brunauer-Emmett-Teller (BET) [30] and Barrett-Joyner-Halenda (BJH) [31,32] calculations were used respectively for the analyses of specific surface area and pore volume data.

2.4.5 Colorimetric analysis

The colorimetric coordinates L*, a* and b* in the CIE 1976 colour space were measured using a portable X-Rite SP60 spectrophotometer. For each sample, 5 different areas were analysed, and the results are reported as average ± standard deviation.

2.4.6 Cup test

Water vapour permeability was tested by readapting a standard protocol already reported in the literature [33]. Formulation A, B and C were cast in cylindrical molds to obtain disk-like specimens (diameter 5.5 cm and height 2 cm), which were cured up to reaching a constant weight (variations < 0.1%). Each specimen was then mounted on a glass cup containing an aqueous saturated salt solution (KNO_3) (wet cup, RH: 93% at 23 °C) and sealed with wax, to prevent any water transfer from the edges. A saturated aqueous solution of $Ca(NO_3)_2$ (RH: 50% at 23 °C) was placed in the chamber together with the wet cups, and the weight of the cups was daily monitored for two weeks. According to the cup test standard [33], it is possible to calculate the water vapour permeance (W_p) with respect to partial vapour pressure ($kg/(m^2 s\ Pa)$):

$$W_p = \frac{G}{A \cdot \Delta p_v}$$

where G is the water vapour flow rate through specimen (kg/s), A is the test surface area (m^2) and Δp_v is water vapour pressure differences across the specimen (Pa). G can be calculated from the slope of the plot of the sample's weight (kg) vs time (seconds), being:

$$G = \frac{|\Delta m|}{\Delta t}$$

11

while Δp_v is calculated from the mean of the temperature and relative humidity measured over the course of the test (water p_v = 28131 Pa at 23 °C).

The water permeability ∂p (kg/(m·s·Pa)) can be then calculated using the formula:

$$\partial p = W_p \cdot D$$

where D is the thickness of specimen (m).

2.4.7 Sponge test

Sponge test [34] was conducted using the contact sponge kit provided by C.T.S. and following the protocol reported by the producers. Formulations A, B and C were cast in parallelepiped-like molds (5x5x2 cm) and cured for 28 days. The obtained specimens were tested, and the time of contact between the samples and the wet sponge, filled with 5 mL of water, was 60 s. The water permeability Wa (g/m^2·s) was calculated using the formula [34]:

$$W_a = \frac{\Delta m}{A \cdot t}$$

where Δm is the mass change, A is the sponge area (0.002376 m^2) and t is the contact time. The values were calculated in three replicas for each formulation.

2.4.8 Shrinkage test

The shrinkage test was performed by curing the fresh pastes in a brass ring of 10 cm of diameter, following a procedure reported in the literature [35]. After drying, when the shrinkage was completed, the presence or the absence of cracks on the sample was noted through a visual inspection.

2.4.9 Peeling test

The peeling test was performed by placing a piece (2 cm x 2 cm) of adhesive tape (3M) on the surface of the specimens, which was smoothened with fingers and firmly rubbed. After 90 s, the tape was removed by seizing the free end and pulling it off rapidly back upon itself [36]. The piece

of tape was weighted before and after the application to estimate the released material. For each sample, three replicas were performed.

2.4.10 Shear adhesion test

The adhesion test was performed by readapting a protocol reported in the literature [37]. Cylindrical plastic molds (diameter 0.9 cm) were filled with fresh pastes and applied on the surface of cured mortars. After 7 and 28 days, the samples were loaded until failure by progressive increments of the applied shear load. The mass at which the sample breaks, which is called failure mass, was recorded and the average shear strength (max, N/mm^2) was calculated as follows:

$$T = m_f \times \frac{g}{S}$$

where m$_f$ is the failure mass (kg), g is the gravitational acceleration (9.81 m/s^2) and S is the surface area of the specimen (mm^2).

2.4.11 Chemical degradation

The resistance of the formulations to chloride penetration was conducted by immersing the samples for 48 h in a saturated solution of NaCl and drying them at 105 °C for 24 h. After 4 cycles (48 h immersion + 24 h at 105 °C), samples were axially broken and the penetration of chloride was evaluated by spraying a solution on AgNO$_3$ (1 M) on the surfaces of the freshly broken samples. The chloride penetration depth is evidenced by the precipitation of white AgCl [38].

2.4.12 Rain test and BTA release

The release of BTA from HNT nanotubes was evaluated by means of a rain test experiment. Fresh pastes of samples A, B and C were applied as coatings on the top of cement mortar samples (diameter 0.7 cm, height 0.5 cm) and cured for 7 and 28 days. Afterwards, the samples were subjected to a simulated moderate rain (5 mm/h [39]) for 1 h, by pouring on the top the adequate amount of water every 5 min. Specimens were then broken, to obtain fragments of the top (coating)

13

and of the bottom (mortar); these fragments were incubated in water for 24 h (using 25 µL of water *per* mg of sample), to completely release the BTA present in the matrix. The amount of released BTA was quantified by means of UV spectroscopy. Samples were analyzed in quartz cuvettes with a Cary3500 (Agilent) in the range 200-800 nm, with an integration time of 0.5 s and a bandwidth of 1 nm. Prior to the measurement, a calibration line of BTA in water was acquired: the absorbance of BTA was measured at 274 nm and we found that $A = 1.21 \cdot c$, where c is the concentration of BTA (mmol/L).

3. Results

3.1 Preliminary experiments

In the design of materials for the restoration of damaged concrete-based historical monuments, several factors should be taken into account: depending on the site of application and on the type of damage to be addressed, it is important for the material to have a proper workability and setting time, and a good adhesion with the substrate where it is applied. As outlined in the Introduction, the goal of our work is to prepare three distinct formulations, each designed for a different type of application, *i.e.*:

A. For delamination problems;

B. For small cracks (width < 5 mm);

C. For big cracks (width 5-10 mm).

Formulation A, to be used in case of delamination problems, was optimized to ensure not only a good adhesion but also an easy spreading, and a smooth appearance. Formulations B and C, to be used in cracks, were optimized to obtain more compact pastes, which would easily fill the voids. In case of smaller cracks (< 5 mm), we decided to prepare a cement paste, not containing sand

14

(formulation B), which can be also injected through a syringe. In case of bigger cracks (5 - 10 mm), a mortar was formulated (formulation C), which could be used not only to repair cracked surfaces, but also to easily reconstruct small detachments, thanks to its plastic behaviour. Figure 1 shows the appearance of the formulations in the designated type of application.
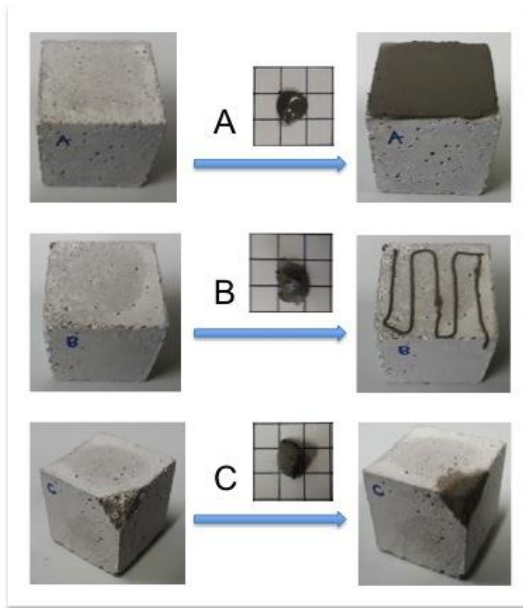

Figure 1. Pictures of freshly prepared formulations and their use in the specific types of application: A spread as a coating, B extruded through a syringe and C applied with a spatula to reconstruct a small damage.

The specific behaviour of the three formulations here discussed was achieved by properly dosing the additives, to address the three very common types of applications that we selected. The final formulations identified are the result of an extensive work devoted to understand the effect of admixtures and of type of silica used in the formulation on the most important properties of the materials. A basic cementitious paste can be prepared by mixing cement, water and, in case of mortars, sand; nevertheless, different types of admixtures are commonly used to tailor the properties of both the paste and the final material. Superplasticizers allow for the obtainment of the desired workability with a reduced amount of water that would be detrimental for the

mechanical properties of the final material. Cellulose ethers can provide water retention, workability and cohesiveness to mixtures, whereas anti-shrinkage agents are commonly used to reduce the shrinkage that can occur during cement curing. Silica also plays a major role in cementitious formulations, as it improves their attachment to the substrate as well as the microstructure of the final products by refining the pore structure [17].

Table S1 and Table S2 in the Supplementary Material report all the formulations prepared by varying the amounts of admixtures and different type/amount of silica. These pastes were evaluated in terms of workability, injectability/ease of application and setting time. The most promising ones (see Figure S1 and Figure S2) were then applied on the surface of reference mortar samples and, after 7 and 28 days of curing, samples were broken to study the ITZ by means of SEM, in order to qualitatively evaluate the adhesion. The micrographs shown in Figure S3 and S4 reveal that a good bonding between the coating and the underneath mortar can be achieved when silica is present in the formulation, suggesting promising properties of these materials. On the basis of the obtained results in terms of workability, setting time and adhesion, three formulations with different consistencies and features were selected to address the different types of damages (A for delamination, B for small cracks and C for large cracks, see the composition in Table 1). HNTs loaded with BTA were included in the three formulations to endow them with anti-corrosive properties.

3.2 Characterization of formulations A, B and C

The nature of the phases formed in the cements was characterized by means of XRD and TGA analyses. In both cases, samples hydrated for 7 and 28 days did not show any significant difference (see Figure S5 and Figure S6), thus only results of the 28 days-cured cements are discussed. The

diffractograms are reported in Figure 2A: all patterns show the peaks characteristic of portlandite ($Ca(OH)_2$), alite (Ca_3SiO_2), belite (Ca_2SiO_2), hemicarboaluminate and ettringite [40–42]. The aforementioned phases demonstrate the formation of a cementitious material: in fact, when mixing cement powders with water, alite and belite are consumed and the formation of crystalline portlandite occurs, together with amorphous calcium silicate hydrate (C-S-H) [1,43]. The presence of C-S-H in our materials is demonstrated by the broadened peak slightly below 30°, diagnostic of this phase [44]. This peak is less evident in sample C, where sand accounts for most of the volume and therefore C-S-H network is less extended. The signals typical of calcite ($CaCO_3$) are also present, due to the carbonation that likely occurs as a consequence of the preparation procedure, or during samples curing [45]. No significant differences among the samples are present, except for the intensification of quartz signals in sample C, due to the presence of sand in the formulation [46].
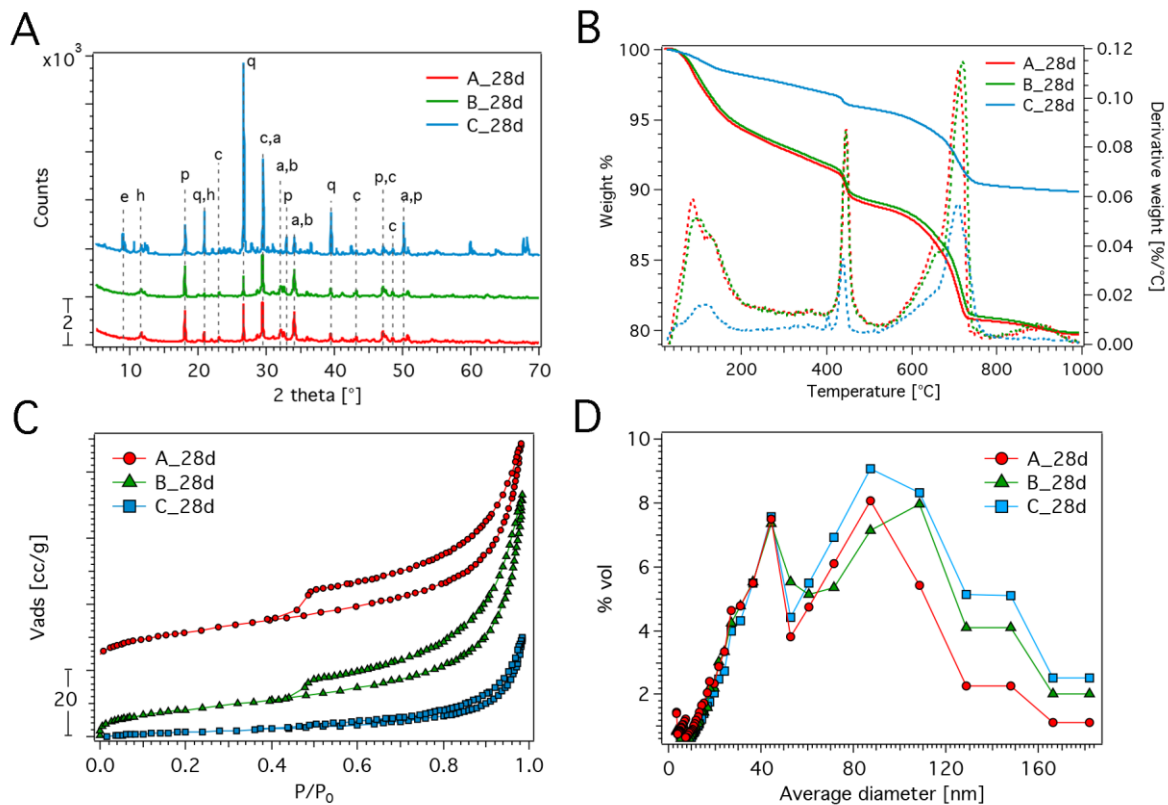
Figure 2. A) XRD patterns of (from the bottom to the top) sample A, B and C after 28 days of hydration. The assignment of the peaks is reported in the figure using the following abbreviations: e (ettringite), p (portlandite), h (hemicarboaluminate), b (belite), a (alite), c (calcite), q (quartz). Curves are offset for the sake of clarity. B) TGA (solid lines) and DTG (dashed lines) curves of the three samples at 28 days of hydration. C) Nitrogen adsorption/desorption isotherms of (from the top) sample A, B and C. The curves are offset for display purposes. D) Pore volume distribution calculated with BJH method.

Thermal analysis results are shown in Figure 2B: the derivative thermogravimetric curves (DTG) reveal that, when heated up to 1000 °C, samples' weight loss mainly occurs in three stages, *i.e.* below 200 °C, at about 430 °C and at 500-800 °C. The first signal is due to water loss, both the adsorbed one and that due to hydrated phases. This signal is less intense in sample C, where sand accounts for most of the volume. The weight loss located around 430 °C corresponds to the dehydroxylation of portlandite, a phase already detected by means of XRD, and confirms the occurrence of the reaction of hydration and the formation of C-S-H binder gel phase. The weight loss between 500 and 800 °C is ascribed to the decomposition of carbonated phases [47] and, only

for sample C, to the degradation of impurities present in the sand used to prepare this mortar (see Figure S7). It is worth mentioning that this non-negligible amount of carbonated phases in our formulations, already detected in XRD analysis, might impact the long term durability, porosity and mechanical properties of the materials [48]: nonetheless, it is important to keep in mind that these formulations are intended to repair and restore small damages in concrete-based monuments rather than to provide structural reinforcement. Samples A and B also display a small peak in the 800-1000 °C range, due to the dehydroxylation of the silanol groups when the transformation of C-S-H to wollastonite ($CaSiO_3$) and SiO_2 occurs [44]. The study of porosity is particularly important when characterizing cement pastes and mortars because it affects the transport properties that in most degradation mechanisms govern the rate of damage [49,50]. By means of nitrogen sorption measurements, we measured the specific surface area and the pore size distribution of the three selected formulations. Figure 2C shows the adsorption/desorption isotherms at 28 hydration days, whereas the pore volume percentage distribution is displayed in Figure 2D. Data obtained for samples cured for 7 days are reported in Figure S8 in the Supplementary Material. The parameters obtained from the analysis are reported in Table 2.

Table 2. Specific Surface Area and Total pore volume of the formulations after 7 and 28 days of hydration.

	SSA (m^2/g)		Total pore volume (mL/g)	
	7 days	28 days	7 days	28 days
A	42.2	38.3	0.13	0.10
B	39.6	30.0	0.10	0.10
C	14.7	10.3	0.05	0.04

All the physisorption isotherms are compatible with macroporous systems of Type II [51,52], and the hysteresis loops can be classified as Type H3, which is associated with capillary condensation [51]. The isotherms are compatible with the existence of aggregates that give rise to polydisperse porosity in the range from micropores to macropores [53]. As it is shown in Figure 2D, most of the pores show a diameter of 40 nm and 100 nm and the dimensions of the pores do not change between 7 and 28 days, even though the matrix is still evolving, as confirmed by the slight decrease in the SSA for the three formulations (see Table 2). The lower surface area of C is due to the presence of sand that accounts for most of the volume in the formulation. It is worth mentioning that only porosities at the nano-scale, which are largely due to the C-S-H network, are accessible with this technique, and the obtained SSA and pore volume are therefore not affected by the possible presence of large micrometric pores.

In addition to the physico-chemical properties of the formulations, the colour of these repair materials is an important parameter. For this reason, the formulations were characterized by means of colorimetric analysis, and the obtained results are reported in Table 3. As expected, quite large standard deviations are associated to the obtained coordinates, due to the inherent inhomogeneities of cementitious materials. According to procedures commonly used for concrete restoration, the colour variation induced by the intervention requires a pictorial retouching, recommended only after 28 days of curing.

Table 3. Colorimetric analyses of the cement formulations at 28 days.

	28 days		
	L*	a*	b*
A	48.2±0.8	-0.54±0.08	4.32±0.47

B	55.5±1.0	-0.56±0.03	4.42±0.29
C	57.0±0.9	-0.03±0.08	6.56±0.66

The ingress of water, eventually together with harmful substances, into the structure of cement-based buildings is one of the main factor affecting the structure lifetime [54]. For these reasons, we performed some experiments to test both water permeability and water adsorption of our formulations. The results of the cup test experiment (see the experimental procedure in section 2.4.6) are reported in Figure 3A and show a different vapour flow rate of the samples, due to the different slope of the lines. In fact, the higher is the slope, the faster is the water vapour transfer from the sample wet cup to the dry cup, revealing a higher vapour permeance of the cement matrix. Experimental data were fitted with a line (see Figure 3A) and the parameters obtained with the calculations reported in section 2.4.6 are shown in Table 4: sample C is the one that shows the highest water vapour permeance and permeability, while the features of A and B are similar, even if B displays a slightly lower Wp and ∂p than A. The obtained permeabilities are about one order of magnitude smaller than those reported for different types of concrete, such as hemp concrete [55] or autoclaved aerated concrete [56]. The increased resistance to vapour permeability might slow down the degradation of the substrate to be protected but could also be detrimental if the surface is not carefully cleaned before applying the repair materials, as it could trap potentially harmful substances already present on the aged surface.
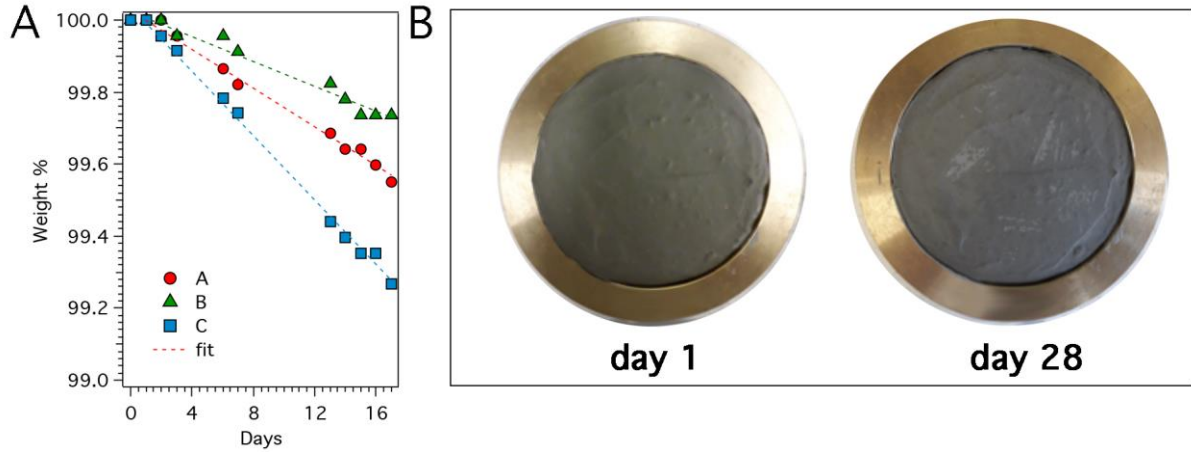
Figure 3. A) Cup test plot (weight % of the cup containing the sample vs days). B) Shrinkage test results for sample A (ring diameter: 10 cm).

Table 4. Parameters obtained from cup test (G: water vapour flow rate, Wp: water vapour permeance, ∂p: water permeability), sponge test (Wa: water absorption) and peeling test (amount of sample dethatched by peeling).

	Cup test			Sponge test	Peeling test	
	G	Wp	∂p	Wa	7 d	28 d
	(kg/s)	(kg/(s·m²·Pa))	(kg/(s·m·Pa))	(g/m²·s)	(mg/cm²)	(mg/cm²)
A	$6.9523\cdot10^{-10}$	$2.93\cdot10^{-11}$	$5.86\cdot10^{-13}$	0.25±0.08	0.035±0.018	0.015±0.010
B	$4.5168\cdot10^{-10}$	$1.90\cdot10^{-11}$	$3.80\cdot10^{-13}$	0.26±0.03	0.033±0.015	0.023±0.018
C	$1.2011\cdot10^{-9}$	$5.06\cdot10^{-11}$	$1.01\cdot10^{-12}$	0.18±0.04	0.073±0.013	0.013±0.010

The water absorption of the formulations was assessed by means of a sponge test (see the experimental details in section 2.4.7), and the results are reported in Table 4: again, sample A and B do not display significant differences, whereas C has an inferior capability of absorbing water for capillarity, consistently with nitrogen sorption data reported in Table 2 which reveal that C has a lower specific surface area and total pore volume than the other two samples. The slightly lower water absorption of C when compared to A and B can be associated with the presence of sand. As a matter of fact, we used a sand of very small granulometry to prepare mortar C, which should be

well suited for filling cavities and cracks, and we obtained quite a compact structure as confirmed by the value of total pore volume (Table 2). In general, all the formulations here discussed present a very low water absorption capability, as in the literature it was reported that mortars prepared using Portland cement and white sand have the capability of absorbing about 7 g/m^2s when performing the contact sponge test for 90 s [34]. As a comparison, our results are similar to silanised marble surfaces [57].

Before applying these repair materials as coatings or to fill cracks, it is important to evaluate if a shrinkage of the cements occurs upon drying: this would in fact lead to the formation of cracks and defects on the material, that would potentially damage the restored area. Fresh pastes were thus cured in 10 cm brass rings and visually inspected up to 28 hydration days. As an example, the results of sample A are shown in Figure 3B, while all samples can be observed in Figure S9. In any case, no shrinkage was observed, proving the potential of these materials. Further encouraging results were obtained with the peeling test, which quantitatively assess the adhesion of the surface layer. The results, reported in Table 4, reveal that a very small amount of material (less than 0.1 mg/cm^2) is detached, which means that the materials are very compact both after 7 and 28 days of hydration. We found an insignificant removal of materials in all cases, similarly [58] or even better [59] than comparable mortars.

3.3 Adhesion of the formulations on cured mortars

The adhesion of the formulations to the surface of the mortars to be repaired was investigated through adhesion test and SEM analyses of the top coating/bottom matrix interphase.

In order to gain quantitative information on the bonding of the top coating to the aged bottom surface, we used the shear resistance test (described in paragraph 2.4.10) [37]. The adhesive

strength was quantified in terms of shear resistance by measuring the weight necessary to remove a sample attached to a standard mortar through a known surface area of contact. The results of the shear resistance test after 7 and 28 days are reported in Figure 4 and we observed a good adhesion of the samples [60,61]. The high adhesion strength of the formulation C is particularly important in view of conservative reconstructions, where lacking parts of the monuments are *de novo* remodelled (as in figure 1C).
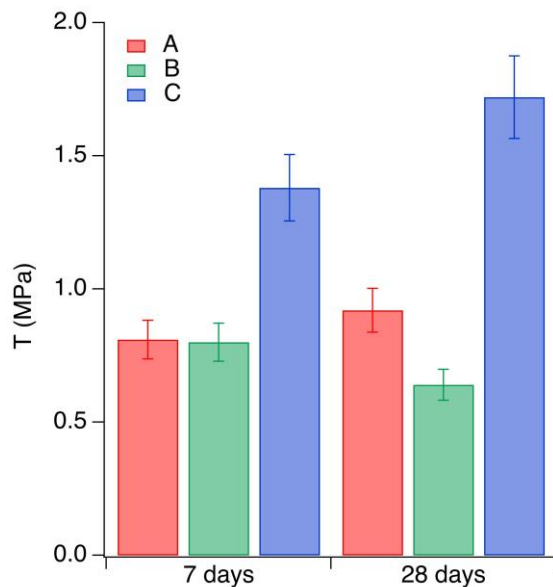

Figure 4. Average shear adhesion strength of the formulations after 7 and 28 days of hydration.

The evaluation of the morphology of the top coating/bottom matrix interphase performed by SEM (Figure 5), allows the study of the bonding of the coating to the aged mortar surface. When breaking the samples in the transverse direction to the interphase, we easily obtained pieces displaying the ITZ between the coating and the matrix, and we observed that the top coating was well attached, as it did not preferentially separate from the bottom matrix. The morphology of the ITZ was studied both in terms of phase attachment and compactness differences between the top coating and the bottom [17]. Looking at Figure 5 it is evident that the interphases (evidenced in

figure with red dotted lines) can be hardly distinguished and we did not evidence differences in terms of morphology and compactness between the coating formulations and the reference mortars. These results confirmed that the proposed formulations present a good adhesion to mortar surfaces.
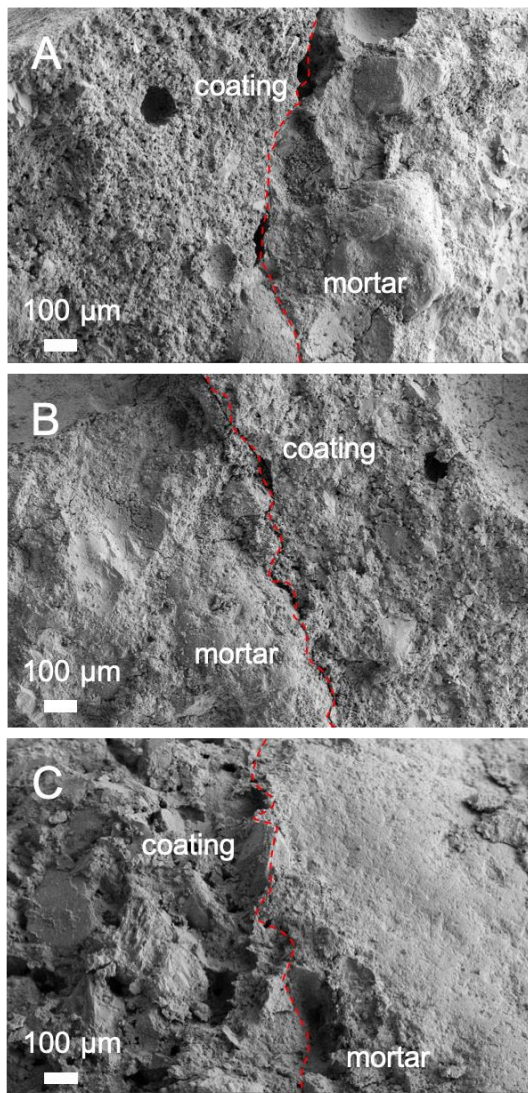

Figure 5. SEM images of the top coating/bottom mortar interphases after 28 days of hydration.

3.4 Resistance to chlorides

The resistance to chlorides penetration was studied through chemical degradation test (described in paragraph 2.4.11), to monitor the migration of chloride anions into the porous structures. Figure 6 shows the samples before and after spraying $AgNO_3$, and the chloride penetration depth is evidenced by the precipitation of white AgCl. Looking at Figure 6, it is evident that for samples A and B we could measure the penetration depth of chloride, which was about 0.2 cm for both samples, while in sample C the chloride penetration occurred in the entire sample. A penetration depth of about 0.2 cm for 8 days of immersion in NaCl solution was already reported for mortars and it has been also stated that the presence of 10 wt% of HNTs improves the resistance to chloride penetration [62]. Taking into account that sample C is a mortar, while samples A and B are cement pastes, this result was not unexpected, and it underlines that formulations A and B are denser than the mortar C. Despite the lower SSA, sample C likely presents a more porous structure, with pores in the micrometric range, as the presence of macropores can be observed also by naked eye (see Figure 6). Therefore, when immersed in chloride solution, in this case Cl$^-$ ions can penetrate the whole structure, pointing out that when using repair mortars, such as formulation C, it is particularly useful to further protect the materials by incorporating corrosion inhibitors and/or using protective coatings.

Figure 6. Results of the chemical degradation for the formulations before and after the test. Samples were tested after 28 days of curing.

It is important to recall here that the presence of corrosion inhibitors loaded into HNTs is also fundamental for the protection of the steel rebars embedded in the cementitious materials against chloride. The evaluation of BTA release was used as an indirect way to study the prevention of the chloride-induced degradation, by looking at the delivery and transport of BTA through the cement matrix. The amount of BTA in the formulations was quantified both in the top coatings ("t" in Figure 7) and in the bottom reference mortars ("b" in Figure 7). Looking at Figure 7 we observe that BTA can be released from HNTs and migrate from the coating to the cement matrix when the surface is exposed to rain, as the concentration of BTA in the top diminishes while that in the bottom increases due to rain effect (note that some BTA leaks out with the rainwater, decreasing the total amount found in the top and bottom after 1 h rain). Thus, HNTs can be effectively used to carry and release the corrosion inhibitors from the repair formulations to the surface of applications.
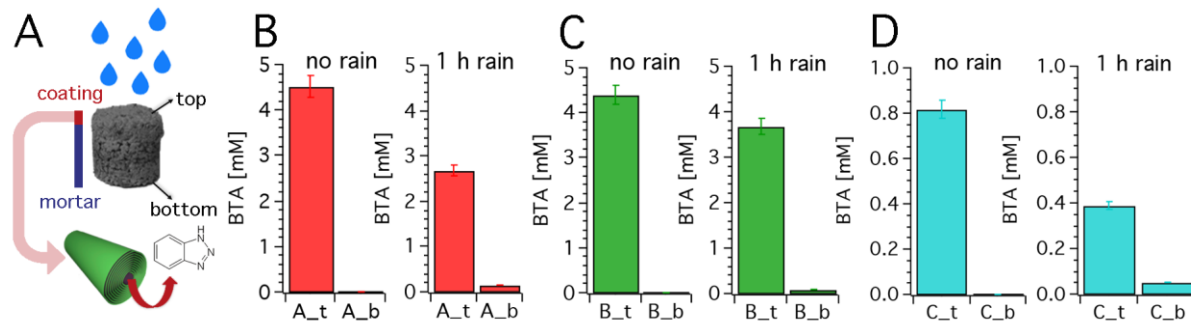

Figure 7. Rain test results for the 1 h rain experiment on the formulations after 7 days of curing. "t" indicates the top, while "b" indicates the bottom of the specimens.

3.5 Applications in real case studies

Following a complete laboratory validation, these innovative formulations were tested in-situ. The site used for the applications is the War Memorial of Torricella Peligna (Italy), that includes two

monuments, "The Angel" and "The Tower", built to commemorate the fallen of the first and second World War, respectively. The figure of the Angel, entirely in concrete, was built in 1922 and is a symbol of victory over the Hapsburg Empire. The Angel was severely damaged first by a hurricane and then by bombing during the Second World War, and the present damages include paint detachment, cracks, delaminations, steel corrosion. The Tower, inaugurated in 1961, is about 20 meters high, entirely made of concrete, with a base of chiselled stone. The interior presents many damages, including small and big cracks, detachments, and corrosion of steel rebars. Formulations A, B and C were used to repair different types of damages, and the pictures before application and the day following the application are shown in Figure 8. Formulation A was used to recover some detachments in the head of the Angel and on the surface of a pillar of the Tower (see Figure 8A), formulation B was used to restore some small cracks inside the Tower (see Figure 8B), and formulation C was used to restore bigger cracks and small damages in the Tower interior (see Figure 8B and 8C). The preliminary results are very promising, as all formulations could be very easily applied in the selected areas and were very effective in repairing cracks and delaminations. In particular, in the case of formulation A and B, it is almost impossible to distinguish the site where the repair product was applied. Moreover, the applications were monitored in time, displaying excellent stability for several months.
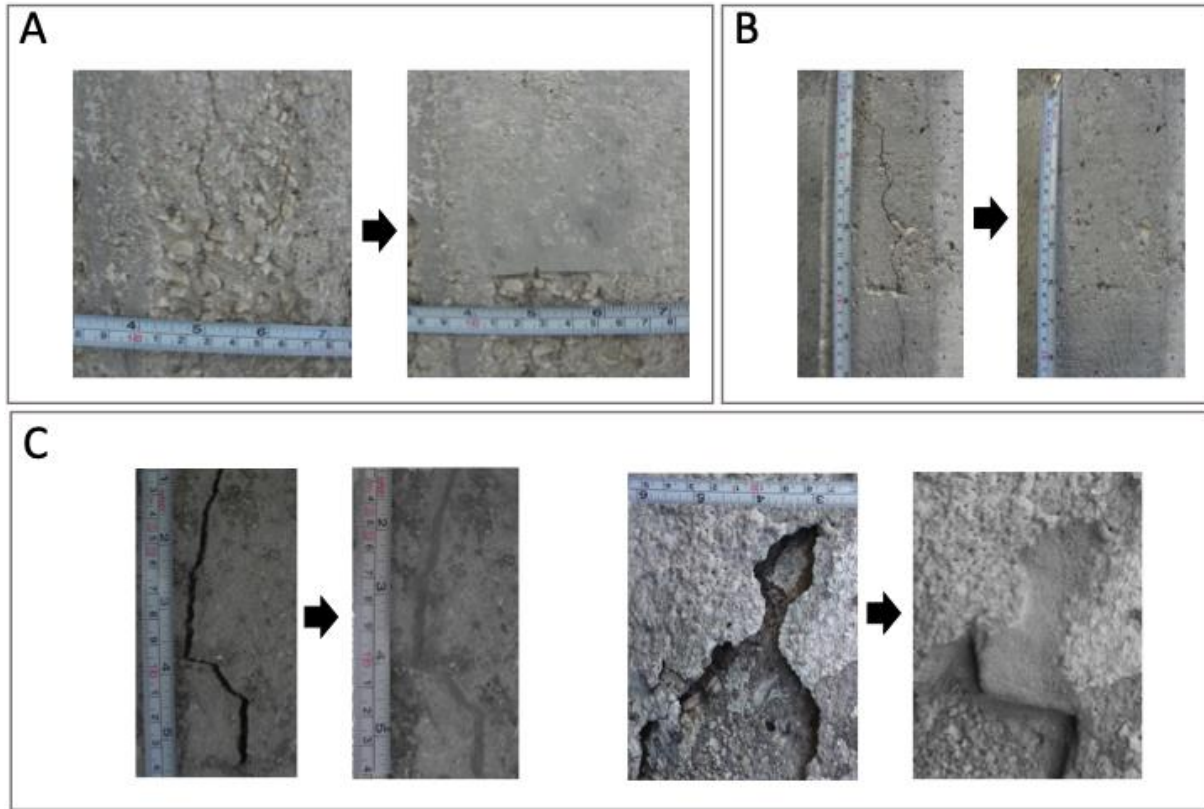
Figure 8. Pictures of the formulations used in the preliminary in-situ applications at Torricella Peligna War Memorial, before and the day after the application. Formulation A was used on the surface of a pillar of the Tower, B was used in a small crack inside the Tower, C was used in a big crack and to reconstruct a small damage in the Tower.

4. Conclusions

In this study we developed three different formulations to address the repair of diverse common types of damages that affect cement-based monuments, *i.e.* delamination problems, cracks of different size and small detachments. Formulation A was optimized to be easily spread as a coating, formulation B was ideated to be extruded through a syringe and used in cracks thinner than 5 mm, and formulation C was designed for an easy application in cracks of 5 – 10 mm and to reconstruct small damages. The three proposed cement-based formulations were designed

incorporating silica, to improve the attachment of the patch repair to the surface to be restored, and halloysite nano-carriers, which can provide a slow release of active molecules and prolong the protective effect of these molecules. Here, halloysites were loaded with benzotriazole, a corrosion inhibitor, to address the problem of steel rebars corrosion, but these nanotubes could be used to carry many other active molecules (such as other corrosion inhibitors or antifouling agents), opening many possibilities in the field of concrete protection. All formulations were thoroughly characterized with a multi-technique approach. Based on the results, we obtained an adequate formation of dense cementitious materials, good adhesion, proper workability and setting time, no shrinkage, and we observed that benzotriazole can be effectively carried and released from the repair formulations to the surface of applications. Following these promising results, the formulations were successfully used to fix some damages at the War Memorial of Torricella Peligna (Italy), demonstrating their potential in the repairing and conservation of concrete-based monuments.

REFERENCES

[1]   A.J. Allen, J.J. Thomas, H.M. Jennings, Composition and density of nanoscale calcium–silicate–hydrate in cement, Nat. Mater. 6 (2007) 311–316. https://doi.org/10.1038/nmat1871.

[2]   F. Ridi, E. Fratini, P. Baglioni, Cement: A two thousand year old nano-colloid, J. Colloid Interface Sci. 357 (2011) 255–264. https://doi.org/10.1016/j.jcis.2011.02.026.

[3]   World Heritage List, https://whc.unesco.org/en/list/?search=20th+Century&.

[4]   L. Bertolini, M. Carsana, M. Gastaldi, F. Lollini, E. Redaelli, Corrosion assessment and restoration strategies of reinforced concrete buildings of the cultural heritage, Mater. Corros. 62 (2011) 146–154. https://doi.org/10.1002/maco.201005773.

[5]   A. Custance-Baker, S. Macdonald, Conserving Concrete Heritage: An Annotated Bibliography. Los Angeles: Getty Conservation Institute (2015).

[6]   J. Valença, C. Almeida, E.S. Júlio, Concrete heritage: Tentative guidelines for the 'Patch Restoration Method' (2012).

[7]   S. Macdonald, A.P.A. Gonçalves, Conservation Principles for Concrete of Cultural Significance (2015).

[8]   L. Bertolini, M. Carsana, E. Redaelli, Conservation of historical reinforced concrete structures damaged by carbonation induced corrosion by means of electrochemical realkalisation, J. Cult. Herit. 9 (2008) 376–385. https://doi.org/10.1016/j.culher.2008.01.006.

[9]   C.U. Grosse, Advances in Construction Materials, Springer, Stuttgard, 2007.

[10]   M. Ibrahim, A.S. Al-Gahtani, M. Maslehuddin, A.A. Almusallam, Effectiveness of concrete surface treatmentmaterials in reducing chloride-induced reinforcement corrosion, Constr. Build. Mater. 11 (1997) 443–451. https://doi.org/10.1016/S0950-0618(97)00023-8.

[11]   A. James, E. Bazarchi, A.A. Chiniforush, P. Panjebashi Aghdam, M.R. Hosseini, A. Akbarnezhad, I. Martek, F. Ghodoosi, Rebar corrosion detection, protection, and rehabilitation of reinforced concrete structures in coastal environments: A review, Constr. Build. Mater. 224 (2019) 1026–1039. https://doi.org/10.1016/j.conbuildmat.2019.07.250.

[12]   W.G. Smoak, Guide to concrete repair, United States department of the interior bureau of reclamation, Books for business, New York - Hong Kong, 2002.

[13]   L. Basheer, J. Kropp, D.J. Cleland, Assessment of the durability of concrete from its permeation properties: a review, Constr. Build. Mater. 15 (2001) 93–103. https://doi.org/10.1016/S0950-0618(00)00058-1.

[14]   F.H. Wittmann, A.D.A. Wittmann, P.G. Wang, Capillary absorption of integral water repellent and surface impregnated concrete, Restor. Build. Monum. 20 (2014) 281–290. https://doi.org/10.12900/rbm14.20.4-0026.

[15] J. De Vries, R.B. Polder, Hydrophobic treatment of concrete, Constr. Build. Mater. 11 (1997) 259–265. https://doi.org/10.1016/S0950-0618(97)00046-9.

[16] N.Z. Muhammad, A. Keyvanfar, M.Z. Abd. Majid, A. Shafaghat, J. Mirza, Waterproof performance of concrete: A critical review on implemented approaches, Constr. Build. Mater. 101 (2015) 80–90. https://doi.org/10.1016/j.conbuildmat.2015.10.048.

[17] B. Zhang, H. Tan, W. Shen, G. Xu, B. Ma, X. Ji, Nano-silica and silica fume modified cement mortar used as Surface Protection Material to enhance the impermeability, Cem. Concr. Compos. 92 (2018) 7–17. https://doi.org/10.1016/j.cemconcomp.2018.05.012.

[18] B.A. Tayeh, B.H. Abu Bakar, M.A.M. Johari, A.M. Zeyad, The Role of Silica Fume in the Adhesion of Concrete Restoration Systems, Adv. Mater. Res. 626 (2012) 265–269. https://doi.org/10.4028/www.scientific.net/AMR.626.265.

[19] P. Faustino, A. Brás, T. Ripper, Corrosion inhibitors' effect on design service life of RC structures, Constr. Build. Mater. 53 (2014) 360–369. https://doi.org/10.1016/j.conbuildmat.2013.11.098.

[20] D.G. Shchukin, M. Zheludkevich, K. Yasakau, S. Lamaka, M.G.S. Ferreira, H. Möhwald, Layer-by-Layer Assembled Nanocontainers for Self-Healing Corrosion Protection, Adv. Mater. 18 (2006) 1672–1678. https://doi.org/10.1002/adma.200502053.

[21] D.G. Shchukin, H. Möhwald, Smart nanocontainers as depot media for feedback active coatings, Chem. Commun. 47 (2011) 8730. https://doi.org/10.1039/c1cc13142g.

[22] H. Tian, W. Li, A. Liu, X. Gao, P. Han, S.-J. Ding, C. Yang, D. Wang, Controlled delivery of multi-substituted triazole by metal-organic framework for efficient inhibition of mild steel corrosion in neutral chloride solution, Corros. Sci. 131 (2018) 1-6. https://doi.org/10.1016/j.corsci.2017.11.010.

[23] N. Farzadnia, A.A. Abang Ali, R. Demirboga, M.P. Anwar, Effect of halloysite nanoclay on mechanical properties, thermal behavior and microstructure of cement mortars, Cem. Concr. Res. 48 (2013) 97–104. https://doi.org/10.1016/j.cemconres.2013.03.005.

[24] E. Joussein, S. Petit, J. Churchman, B. Theng, D. Righi, B. Delvaux, Halloysite clay minerals - A review, 2005. https://doi.org/10.1180/0009855054040180.

[25] E. Abdullayev, R. Price, D. Shchukin, Y. Lvov, Halloysite Tubes as Nanocontainers for Anticorrosion Coating with Benzotriazole, ACS Appl. Mater. Interfaces. 1 (2009) 1437–1443. https://doi.org/10.1021/am9002028.

[26] E. Abdullayev, Y. Lvov, Halloysite clay nanotubes as a ceramic "skeleton" for functional biopolymer composites with sustained drug release, J. Mater. Chem. B. 1 (2013) 2894. https://doi.org/10.1039/c3tb20059k.

[27] P. Scarfato, E. Avallone, L. Incarnato, L. Di Maio, Development and evaluation of halloysite nanotube-based carrier for biocide activity in construction materials protection, Appl. Clay Sci. 132–133 (2016) 336–342. https://doi.org/10.1016/j.clay.2016.06.027.

[28] M. Sheban, M. Abu-Dalo, A. Ababneh, S. Andreescu, Effect of benzotriazole derivatives on the corrosion of steel in simulated concrete pore solutions, Anti-Corros. Methods Mater. 54 (2007) 135–147. https://doi.org/10.1108/00035590710748605.

[29] H. Yang, W. Li, X. Liu, A. Liu, P. Hang, R. Ding, T. Li, Y. Zhang, W. Wang, C. Xiong, Preparation of corrosion inhibitor loaded zeolites and corrosion resistance of carbon steel in simulated concrete pore solution, Constr. Build. Mater. 225 (2019) 90–98. https://doi.org/10.1016/j.conbuildmat.2019.07.141.

[30] S. Brunauer, P.H. Emmet, E. Teller, Adsorption of Gases in Multimolecular Layers, J. Am. Chem. Soc. 60 (1938) 309–319. https://doi.org/10.1021/ja01269a023.

[31] E.P. Barrett, L.G. Joyner, P.P. Halenda, The Determination of Pore Volume and Area Distributions in Porous Substances. I. Computations from Nitrogen Isotherms, J. Am. Chem. Soc. 73 (1951) 373–380. https://doi.org/10.1021/ja01145a126.

[32] K.A. Kalliopi, Pore Structure of Cement-Based Materials, CRC Press, 2005.

[33] UNI EN 15803 Determination of water vapour permeability, (2010).

[34] D. Vandevoorde, M. Pamplona, O. Schalm, Y. Vanhellemont, V. Cnudde, E. Verhaeven, Contact sponge method: Performance of a promising tool for measuring the initial water absorption, 10 (2009) 41–47. https://doi.org/10.1016/j.culher.2008.10.002.

[35] Bob de Vekey, Andrew Sutherland, Alan Ferguson, A new total shrinkage test for mortar, 9th Canadian Masonry Symposium, in: Fredericton, Canada, 2001.

[36] M. Drdáckỳ, J. Lesák, S. Rescic, Z. Slížková, P. Tiano, J. Valach, Standardization of peeling tests for assessing the cohesion and consolidation characteristics of historic stone surfaces, Mater. Struct. 45 (2012) 505–520. https://doi.org/10.1617/s11527-011-9778-x.

[37] F. Stazi, A. Nacci, F. Tittarelli, E. Pasqualini, P. Munafò, An experimental study on earth plasters for earthen building protection: The effects of different admixtures and surface treatments, J. Cult. Herit. 17 (2016) 27–41. https://doi.org/10.1016/j.culher.2015.07.009.

[38] Concrete, mortar and cement-based repair materials: Chloride migration coefficient from non-steady-state migration experiments, (1999).

[39] Glossary of Meteorology. "Rain". American Meteorological Society., Gloss. Meteorol. (2010). https://web.archive.org/web/20100725142506/http://amsglossary.allenpress.com/glossary/search?id=rain1.

[40] H.-A. Nguyen, T.-P. Chang, J.-Y. Shih, C.-T. Chen, T.-D. Nguyen, Sulfate resistance of low energy SFC no-cement mortar, Constr. Build. Mater. 102 (2016) 239–243. https://doi.org/10.1016/j.conbuildmat.2015.10.107.

[41] M. Tonelli, F. Martini, L. Calucci, M. Geppi, S. Borsacchi, F. Ridi, Traditional Portland cement and MgO-based cement: a promising combination?, Phys. Chem. Earth Parts ABC. 99 (2017) 158–167. https://doi.org/10.1016/j.pce.2017.01.011.

[42] Q. Ye, K. Yu, Z. Zhang, Expansion of ordinary Portland cement paste varied with nano-MgO, Constr. Build. Mater. 78 (2015) 189–193. https://doi.org/10.1016/j.conbuildmat.2014.12.113.

[43] S. Diamond, Hydraulic Cement Pastes: Their Structure and Properties, (1976).

[44] B. Lothenbach, D. Nied, E. L'Hôpital, G. Achiedo, A. Dauzères, Magnesium and calcium silicate hydrates, Cem. Concr. Res. 77 (2015) 60–68. https://doi.org/10.1016/j.cemconres.2015.06.007.

[45] M.S. El-Mahllawy, A.M. Kandeel, M.L. Latif, A.M. El Nagar, The Feasibility of Using Marble Cutting Waste in a Sustainable Building Clay Industry, Recycling 3(3) (2018) 39. https://doi.org/10.3390/recycling3030039.

[46] N. Kouras, A. Harabi, F. Bouzerara, L. Foughali, A. Policicchio, S. Stelitano, F. Galiano, A. Figoli, Macro-porous ceramic supports for membranes prepared from quartz sand and calcite mixtures, J. Eur. Ceram. Soc. 37 (2017) 3159-3165. https://doi.org/10.1016/j.jeurceramsoc.2017.03.059.

[47] Q.T. Phung, N. Maes, S. Seetharam, Pitfalls in the use and interpretation of TGA and MIP techniques for Ca-leached cementitious materials, Mater. Des. 182 (2019) 108041. https://doi.org/10.1016/j.matdes.2019.108041.

[48] B. Šavija, M. Luković, Carbonation of cement paste: Understanding, challenges, and opportunities, Constr. Build. Mater. 117 (2016) 285–301. https://doi.org/10.1016/j.conbuildmat.2016.04.138.

[49] F. Ridi, E. Fratini, P. Baglioni, Fractal Structure Evolution during Cement Hydration by Differential Scanning Calorimetry: Effect of Organic Additives, J. Phys. Chem. C. 117 (2013) 25478–25487. https://doi.org/10.1021/jp406268p.

[50] F. Ridi, P. Luciani, E. Fratini, P. Baglioni, Water Confined in Cement Pastes as a Probe of Cement Microstructure Evolution, J. Phys. Chem. B. 113 (2009) 3080–3087. https://doi.org/10.1021/jp808754t.

[51] Giles, C. H., Anthony, P., Easton, I. A., A General Treatment and Classification of the Solute Adsorption Isotherms-Part II. Experimental Interpretation, 47 (1974) 766–778. https://doi.org/10.1016/0021-9797(74)90253-7.

[52] C.H. Giles, D. Smith, A. Huitson, A general treatment and classification of the solute adsorption isotherm. I. Theoretical, J. Colloid Interface Sci. 47 (1974) 755–765. https://doi.org/10.1016/0021-9797(74)90252-5.

[53] Sing, K. S. W., Everett, D. H., W. Haul, R. A., Moscou, L., Pierotti, R. A., Rouquerol, J., Siemieniewska, T., Reporting physisorption data for gas/solid systems, Pure Appl Chem. 57 (1985) 603–619. https://doi.org/10.1351/pac198557040603.

[54] F. Ridi, M. Tonelli, E. Fratini, S.-H. Chen, P. Baglioni, Water as a Probe of the Colloidal Properties of Cement, Langmuir. 34 (2018) 2205–2218. https://doi.org/10.1021/acs.langmuir.7b02304.

[55] B. Seng, C. Magniont, S. Lorente, Characterization of a precast hemp concrete block. Part II: Hygric properties, J. Build. Eng. 24 (2019) 100579. https://doi.org/10.1016/j.jobe.2018.09.007.

[56] C. Feng, Q. Meng, Y. Feng, H. Janssen, Influence of Pre-conditioning Methods on the Cup Test Results, Energy Procedia. 78 (2015) 1383–1388. https://doi.org/10.1016/j.egypro.2015.11.158.

[57] F. Gherardi, D. Gulotta, S. Goidanich, A. Colombo, L. Toniolo, On-site monitoring of the performance of innovative treatments for marble conservation in architectural heritage, Herit. Sci. 5 (2017) 4. https://doi.org/10.1186/s40494-017-0118-5.

[58] M. Drdáckỳ, J. Lesák, S. Rescic, Z. Slížková, P. Tiano, J. Valach, Standardization of peeling tests for assessing the cohesion and consolidation characteristics of historic stone surfaces, Mater. Struct. 45 (2012) 505–520. https://doi.org/10.1617/s11527-011-9778-x.

[59] M. Drdácký, Z. Slížková, *In situ* peeling tests for assessing the cohesion and consolidation characteristics of historic plaster and render surfaces, Stud. Conserv. 60 (2015) 121–130. https://doi.org/10.1179/2047058413Y.0000000116.

[60] G. Bei, I. Papayianni, Experimental study of shear bond strength of traditional masonry, 13th International Brick and Brick Masonry Conference, Amsterdam, (2004).

[61] Long-term Performance and Durability of Masonry Structures - Degradation Mechanisms, Health Monitoring and Service Life Design, Woodhead Publishing, (2019).

[62] B. Rabehi, Study of calcined halloysite clay as pozzolanic material and its potential use in mortars, Int. J. Phys. Sci. 7 (2012). https://doi.org/10.5897/IJPS11.184.